Journal of Electronic Materials (2024) 53:6124–6139
https://doi.org/10.1007/s11664-024-11358-5

ORIGINAL RESEARCH ARTICLE

Equivalent Circuit Model of Magnetoelectric Composite Nanoparticles

Zeinab Ramezani[1] · **Sakhrat Khizroev**[1]

Received: 27 November 2023 / Accepted: 29 July 2024 / Published online: 16 August 2024

Abstract
This study presents an analysis of magnetoelectric nanoparticles (MENPs) through the development of equivalent circuits to predict the frequency-dependent magnetoelectric coefficient, with a focus on the widely utilized $CoFe_2O_4$@$BaTiO_3$ core–shell configuration. This approach involves –derivation of phenomenological expressions that capture the dynamic behavior of MENPs under varying magnetic and electric fields. By integrating piezoelectric and magnetostrictive constitutive equations, along with consideration of dynamic effects and bio-load conjugation, a magneto-elasto-electric effect equivalent circuit has been constructed. This circuit model not only facilitates the investigation of longitudinal data in cube-shaped MENPs but also offers insights into fundamental biological processes. The versatility of this model is shown through translation to other core–shell nanoparticles, composite structures, and multiferroic nanostructures. This analysis provides quantitative predictions of the magnetoelectric coefficients, enhancing general understanding of MENP characteristics across a broad frequency range. Furthermore, the study highlights the framework for future refinement to incorporate intrinsic composition-specific resonances, such as ferromagnetic and ferroelectric resonances, to further significantly improve the nanoparticles' performance. Overall, this work lays the groundwork for future technology to intelligently and wirelessly control biological processes using MENPs, thus paving a way for innovative biomedical applications. This quantitative approach may facilitate further interdisciplinary research and contribute to advancement of magnetoelectric materials and their applications.

Keywords Magnetoelectric nanoparticles · $CoFe_2O_4$@$BaTiO_3$ · ferrimagnetic · magnetostrictive · ferroelectric · piezoelectric · core–shell nanoparticles · equivalent circuit

Introduction

Nanomedicine is a rapidly emerging application of nanotechnology that is based on the use of multifunctional nanoparticles for molecular-level targeted generation and detection of specific therapeutic responses, thus enabling highly personalized and precision medicine. Owing to the significantly increased surface-to-volume ratio and the presence of quantum-mechanical effects in the nanoscale size range, nanoparticles promise to unlock unprecedented capabilities that could revolutionize the medicine of the future.[1,2]

Among many nanoparticle-based nanostructures being investigated to date, magnetoelectric nanoparticles (MENPs) present their own niche due to the presence of a substantial magnetoelectric (ME) effect.[3,4] Conventionally, the ME effect is defined as the differential coefficient that describes a linear dependence of the polarization (intrinsic electric field) versus the applied magnetic field. Reciprocally, the converse ME effect is defined as the derivative of the magnetization versus the applied electric field. As a result, MENPs represent a very compelling enabler of a two-way wireless control of fundamental biological mechanisms, in turn potentially unlocking a dynasty of unprecedented medical applications. It is noteworthy that electricity is intrinsic to all biological mechanisms.[5] An obvious example is the brain, the most complex organ of the human body, which is made of trillions of electric circuits that are operated by local electric fields. However, because of the mostly conductive biological tissues, cellular-level detection and treatment of neurological diseases and disorders without using surgically implanted electrodes is out of the question. Another important example

✉ Sakhrat Khizroev
skhizroev@miami.edu

Zeinab Ramezani
z.ramezani@miami.edu

[1] Department of Electrical and Computer Engineering, College of Engineering, University of Miami, Miami, FL, USA

relates to controlling the underlying mechanisms of cancers. Arguably, the most fundamental difference between cancer and normal cells lies in their metabolic pathways.[6] To divide, cancer cells require a significantly increased uptake of glucose and rates of glutaminolysis and fatty acid synthesis, compared to healthy cells. In turn, these (cancer and healthy cells) pathways, being determined by electric fields-based molecular couplings, are differently affected by externally applied electric fields. Reciprocally, by generating different local electric fields, cancer and healthy cells can be distinguished from each other if the electric fields can be detected wirelessly. Hence, it would make sense to leverage electric field-based specificity of cellular metabolic pathways to create specificity in controlling cell divisions between cancer and healthy cells. There are many other examples that prove the fundamental significance of the ability to wirelessly control, i.e., write and read local electric fields underlying intrinsic biological mechanisms.[7,8]

However, there is a major stumbling block to achieving such a control. Given that most biological tissues are conductive, electric fields generated by local sources are screened out by free ions in the tissue, thus rendering wireless electric field control of intrinsic biological mechanisms impossible using the electric fields alone. In contrast, magnetic fields easily penetrate both conductive tissues and dielectric bones and other organs, and can be controlled wirelessly with high spatial and temporal precision. In other words, ideally, if electric and magnetic fields could be used together, this could solve some of the most fundamental problems in the quest to regulate intrinsic biological mechanisms. Owing to the ME effect, MENPs provide an answer to this exact open question.

There are two types of MENPs, single-phase and multiphase, such as composite nanostructures. In the former, magnetic and electric fields originate from one phase; though promising, their ME effect, at least as of today, is relatively small, << 0.1 mV/cm/Oe.[9] In contrast, in the latter, magnetic and electric fields originate from two different phases, which are coupled through strain at lattice-matched interfaces; their ME effect can be substantially higher, >1 V/cm/Oe,[10–12] and can be employed for both drug delivery and neuromodulation and neural[13–15] and/or cellular recording.[16,17]

Nanoparticles with a core–shell structure, i.e., belonging to a 0–3 composite material system, such as those made of magnetostrictive (MS) inverse spinel ($CoFe_2O_4$) and piezoelectric (PE) perovskite ($BaTiO_3$), are popular examples of composite MENPs. The unique combination of MENPs' properties makes them highly suitable for nanomedicine applications, as they encompass three essential characteristics to serve as powerful theragnostic agents.[18]

First, owing to the presence of a non-zero magnetic moment, they enable in vivo imaging for disease detection via magnetic imaging instruments such as magnetic resonance imaging, magnetic particle imaging, or others.[19–21] However, owing to the ME effect, being also responsive to local electric fields, the magnetic signal detected by these instruments will contain this additional information due to the electric field modulation, something the traditional purely magnetic nanoparticles do not provide.[20,22,23] Furthermore, using metastable physics allows the nanoparticles to be navigated to a specific place in the brain.[24] According to the U.S. Food and Drug Administration, magnetic fields can be wirelessly controlled without causing damage to the body's electric circuitry as long as the field strength and frequency are kept below the safe limits, which are quite high.[25] Second, owing to the ability to controllably generate local electric fields, these nanoparticles have targeting capabilities that can specifically seek out and penetrate cancer cells.[26] Third, they have the ability to locally electrically stimulate specific cells, if they are placed on the cellular membrane, and/or enable the controlled release of drugs once inside the diseased cells.[27] This local electric-field control, i.e., either to locally stimulate cells or to deliver the required bio-load to a specific target site on demand, is achieved due to the presence of the ME effect via application of magnetic fields.

It can be noted that combining these three characteristics would allow MENPs to be simultaneously used for wirelessly controlled targeted high-precision diagnostic and therapy, thus turning MENPs into a powerful theragnostic tool.[18,28,29] A two-way wireless brain–machine interface (BMI) based on MENPs has already been studied.[22,30] This current study aims to study the MENP properties important for the "write" component of the BMI technology, as well as other applications which have the ability to generate local electric fields in wide ranges of strengths and frequencies, e.g., for the high-specificity stimulation, electroporation of the cellular membrane or targeted drug delivery. The general concept to "write" electric field information with MENPs by application of magnetic fields is illustrated in Fig. 1. Specifically, the purpose of this study is to model MENP properties which would help to understand the dynamic response of the aforementioned applications.

Describing MENPS through circuit modeling would help researchers not only better understand these nanoparticles but also gain insight into the interaction of the nanoparticles with biological microenvironments, thus unlocking their technology potential and allowing the creation of appropriate designs and functions. One major question would be where exactly in the cellular microenvironment do the MENPs need to be placed to achieve the most effective treatment. For example, placing MENPs in a conductive intra- or extracellular space would lead to a significantly stronger field screening effect compared to the case when MENPs are

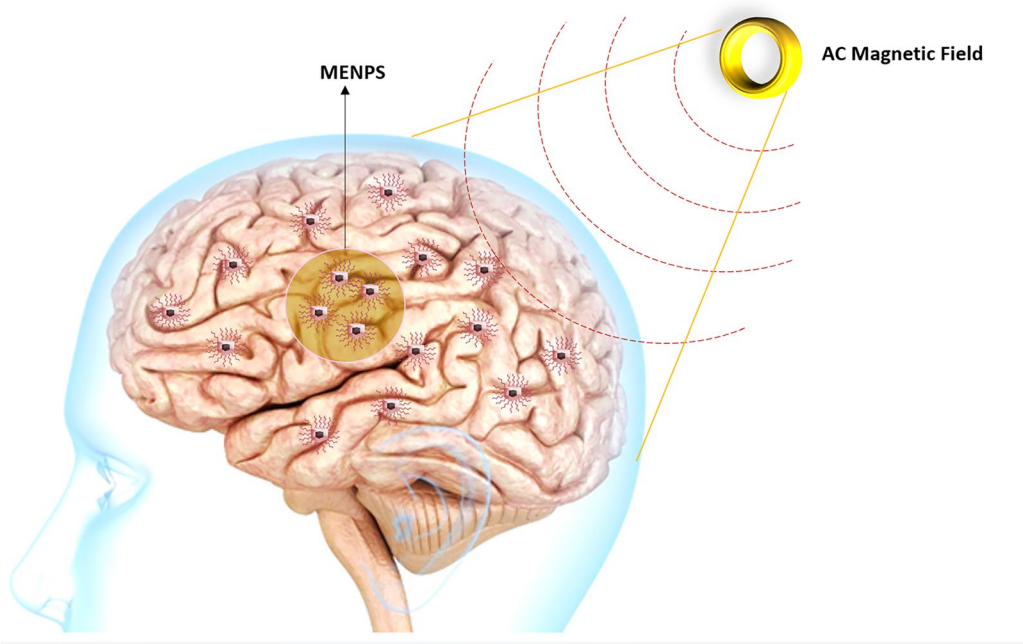

Fig. 1 The use of localized MENPs to "write" information into a specific area deep in the brain. An alternating magnetic field is used to create local electric fields near MENPs that are high enough to set off action potentials.

placed right on the dielectric membrane surface. In this study, the main approach is to design an equivalent circuit for MENPs by coupling MS and PE constitutive equations with an equation of motion. First, the magnetic-mechanical-electric equations are derived from MS and PE constitutive equations and an equation of motion. Then, based on these equations, an equivalent circuit to describe the ME coupling can be derived depending on the MENP's specific location in the cellular microenvironment. The derived equivalent circuit representation of MENPs can be utilized to predict the voltage coefficients of $CoFe_2O_4@BaTiO_3$ composite nanoparticles, which is one of the most important parameters to understand and control MENP properties in the biological body.

Recently, the field of magnetoelectric composites has surged, marked by advancements in magnetic control and the emergence of many innovative applications. Researchers have diligently probed voltage-controlled magnetism across various composite systems, encompassing solid-state and solid–liquid configurations.[31,32] Furthermore, recent studies have unveiled robust magnetoelectric coupling effects in fluid-based magnetoelectric systems like $BaTiO_3@CoFe_2O_4$, promising exciting future applications.[33,34] However, amid these strides, an open question remains in comprehending the dynamic behavior and pragmatic applications of magnetoelectric composites, notably in bridging the divergence between fluid-based and solid-state systems. While scholarly endeavors have shed light on the rheological properties of fluid-based magnetic composites, such as silicone oil-based ferrofluids with nanoparticles and carbon nanotubes,[35,36] further probing is imperative to unravel their mechanical intricacies and to assess their real-world viability. Moreover, the current literature lacks exhaustive studies on anomalous magnetoelectric coupling effects in binary mixed fluids, exemplified by $CoFe_2O_4@BaTiO_3$ systems, which hold the potential to offer fresh insights into underlying phenomena and to guide the evolution of advanced magnetoelectric devices.[37] Hence, the present study endeavors to bridge this gap by undertaking a comprehensive investigation into the magnetoelectric properties of composite nanoparticles and their dynamic response within biological microenvironments. This study fills the gap in the literature by providing a rigorous circuit-based theoretical foundation for understanding MENPs at the nanoscale and exploring their potential applications in healthcare. Through emphasis on theoretical modeling, this research significantly advances the understanding of magnetoelectric phenomena and unlocks the untapped potential of MENPs in medical sciences and biomedical applications. The novelty of this work lies in its innovative approach to model MENPs at the nanoscale, its emphasis on understanding MENPs' interaction with biological microenvironments, and its contribution to advance the theoretical understanding of magnetoelectric materials. It is worth noting that the predictive capabilities of this studied model may be limited by factors such as variations in nanoparticle properties, environmental conditions, and biological responses, though given an important insight to foresee a dynasty of emerging applications.

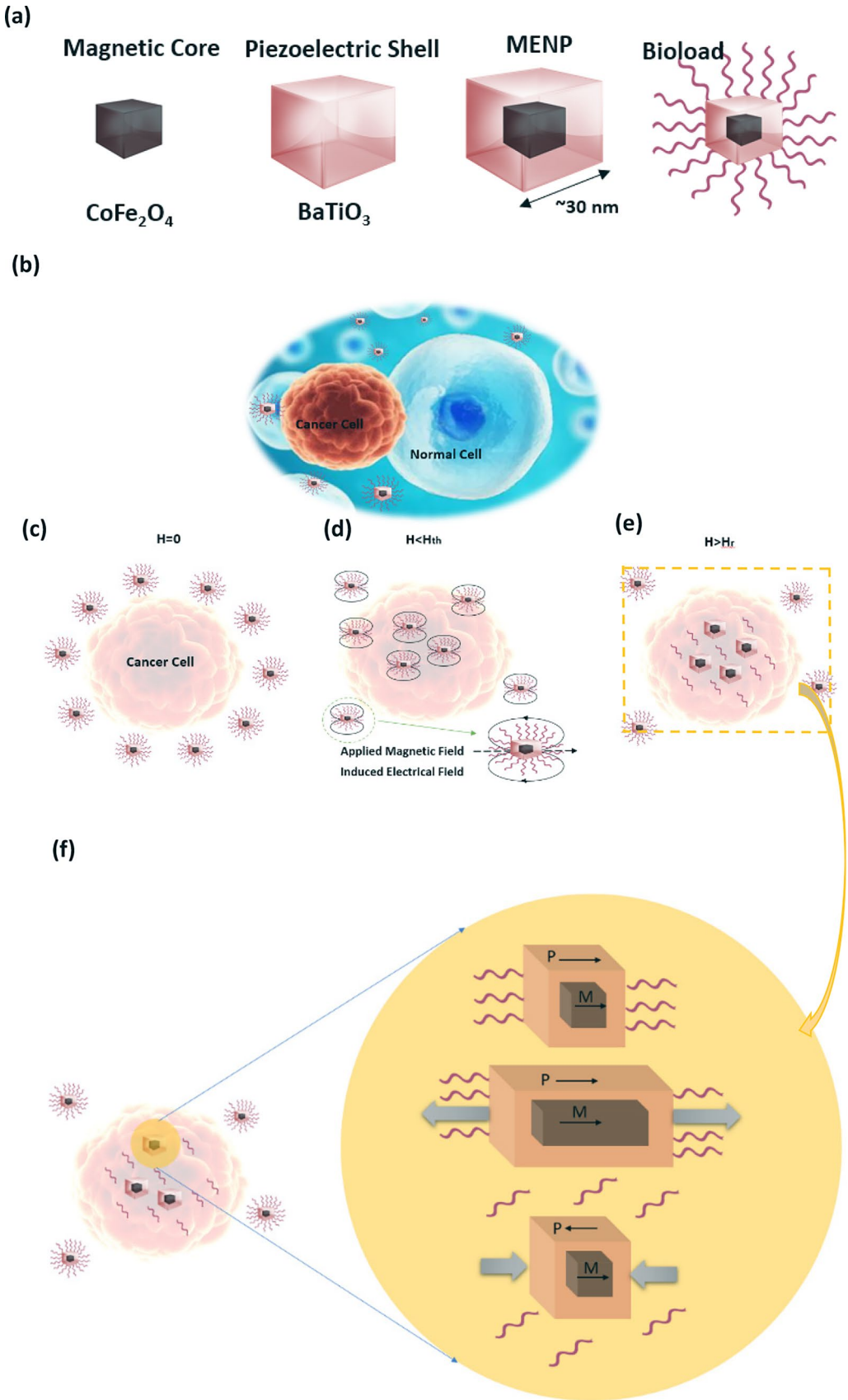
(a)
Magnetic Core
Piezoelectric Shell
MENP
Bioload
$CoFe_2O_4$
$BaTiO_3$
~30 nm
(b)
Cancer Cell
Normal Cell
(c)
H=0
Cancer Cell
(d)
H<Hth
Applied Magnetic Field
Induced Electrical Field
(e)
H>Hr
(f)
P
M
P
M
P
M

◂**Fig. 2** MENP drug delivery platform for treating disease: (a) different layers of the MENP, and (b) part of cancer and normal cells in the body, (c–f) steps of MENPs-based targeted drug release: (c) when $H = 0$, drug-loaded MENPs cannot penetrate to cell membrane from extracellular space, (d) nano-electroporation to penetrate specific cancer cells, (e) on-demand drug release, and (f) schematic of magnetostriction and PE effect on releasing drug. H_{th} and H_r define the cell penetration threshold and drug release fields, respectively.

In summary, the field of MENPs and their applications in medical settings is an actively emerging area of research. Different independent studies have explored different aspects of this topic, though with a strong focus on the experimental side. The focus of this study is to fill the existing gap according to current literature.[1,2] While previous studies have explored magnetoelectric materials and their applications,[4,22,38] this work stands out by specifically modeling MENPs at the nanoscale, developing an equivalent circuit, and considering dynamic effects due to biomolecule conjugation. This theoretical approach, by bridging the gap between microscale composite laminate composites and nanoscale modeling, contributes to the field by expanding the understanding of magnetoelectric phenomena, and even further unlocking the currently untapped potential of these nanostructures in medical applications. In particular, by developing a circuit-based approach, considering dynamic effects, and focusing on medical applications, this research offers valuable insights into the behavior and potential uses of MENPs in healthcare.

Stimuli-responsive MENPs in Drug Delivery

This study focuses on the electric response over a specific bandwidth to the magnitude of an applied alternating current (AC) magnetic field, H_{ac}, on MENPs. Throughout this study, an AC magnetic field is considered the input, and an AC electric field is considered the output of the circuit. The developed model can be applied to any nanomedicine application. For a descriptive purpose, the immediate focus of the model's description is on drug delivery, in which the drug is attached to the core–shell nanostructure. It has been demonstrated that MENPs which have magnetic cores surrounded by PE shells preferentially target cancer cells by creating localized changes in the permeability of the cell's membrane, a high-specificity process known as electroporation, since cancer cells have different membrane potentials compared to that of normal cells.[25] Often, cancer cells have a lower threshold for electroporation and are therefore more permeable when exposed to an electric field. With MENPs, the electroporation process can be scaled down into the nanoscale and also made wireless, thus leading to significantly reduced side effects. An externally applied magnetic field changes the shape of the inner core, due to the phenomenon known as magnetostriction. When a magnetic field is applied, the MS phase experiences strain, which is then transferred to the PE (PE) phase, thus in turn changing the shape of the PE shell. At this stage, electric polarization is induced because of the PE effect. As a result, an electric field is generated in the nanoscale vicinity of the nanoparticle. This electric field in turn can induce the nano-electroporation of the cancer cells, considering that the nanoparticles are right on the membrane. Then, an ideal scenario can be envisioned. Once the MENPs are inside the cancer cells due to the nano-electroporation process, an alternating magnetic field induced by a coil could vibrate the magnetic dipole of the particle and "shake-off" the drug by significantly weakening the electric field bond that holds the two together. In other words, the drug is released off the nanoparticles inside the cancer cells at a specific frequency, sparing the healthy cells from the toxic cancer therapy (Fig. 2). According to earlier experimental papers, there are indications that a relatively small magnitude AC field (50 Oe) in the near-direct current (DC) frequency range of 10 to over 100 Hz could be sufficient to release a significant amount of the drug into the cancer cells.[5,15,17,39,40] However, these experiments are preliminary and do not provide a comprehensive study of the underlying mechanisms. It is noteworthy that, to date, no theoretical study has been conducted to quantify the process.

According to a trivial linear expression, derived from the phenomenological Landau equation for the free energy of magnetoelectric systems, the electric dipole moment induced by an external magnetic field due to the ME effect, would be on the order of $\Delta P = \alpha H$;[41] thus, the displaced surface charge density on the diametrically opposite side of the nanoparticle is $\sigma_{ME}{\sim} \pm \alpha H$. In other words, the electric dipole moment breaks the symmetry of the ionic bonds around the nanoparticle when it is set off by a magnetic field.

When the displaced surface charge is comparable to the charge involved in the original bond, the bond can be broken to a zeroth approximation.[40] The threshold magnetic field amplitude to break a bond can then be calculated using:

$$H_{\text{th}} = \frac{Q_{\text{ionic}}}{\pi d^2 \alpha} \tag{1}$$

where d represents the diameter of the nanoparticle, assuming a spherical shape, α stands for the ME coefficient, and Q_{ionic} stands for the displaced charge in the ionic bond. When an AC field is put around a nanoparticle, it breaks the bonds in every direction. It is worth mentioning that application of external magnetic fields enables MENPs to control the retention of drugs; the first step of high-specificity cellular penetration and the last step of drug release off MENPs are triggered by the application of AC and DC fields, respectively.[40]

Theoretical Analysis and Results

In its most general form, the ME effect is the connection between electric and magnetic fields in matter.[42] The magnetoelectric effect is a "coupled" or "crossed" two-field effect. Application of magnetic and electric fields lead to changes in the nanoparticle's polarization and magnetization, respectively. The ME effect in composite magnetoelectric nanostructures is due to the crystallographic lattice match between adjacent MS and PE components. One popular example is a core–shell configuration made of a $CoFe_2O_4$ ferrimagnetic core and a $BaTiO_3$ PE shell. This configuration is known to display one of the strongest ME values, ~ 1 V/cm/Oe, compared to other core–shell configurations. Our objective is to simulate the properties of this particular configuration.

The shape of the nanoparticles under study was chosen based on Ref. 43 (Fig. 3a). As for their size range, according to a variety of chemical processes, including coprecipitation, thermal breakdown, and others it is possible to adjust the size of $CoFe_2O_4/BaTiO_3$ composite nanoparticles from less than 20 nm to more than 100 nm. Thus, MENPs can be as small as few tens of nanometers in diameter and can be directed throughout the body, including across the blood-brain barrier, and manipulated to preferentially penetrate diseased tumor cells before releasing their drugs. Figure 3b shows a schematic of the core–shell ME nanoparticles. The

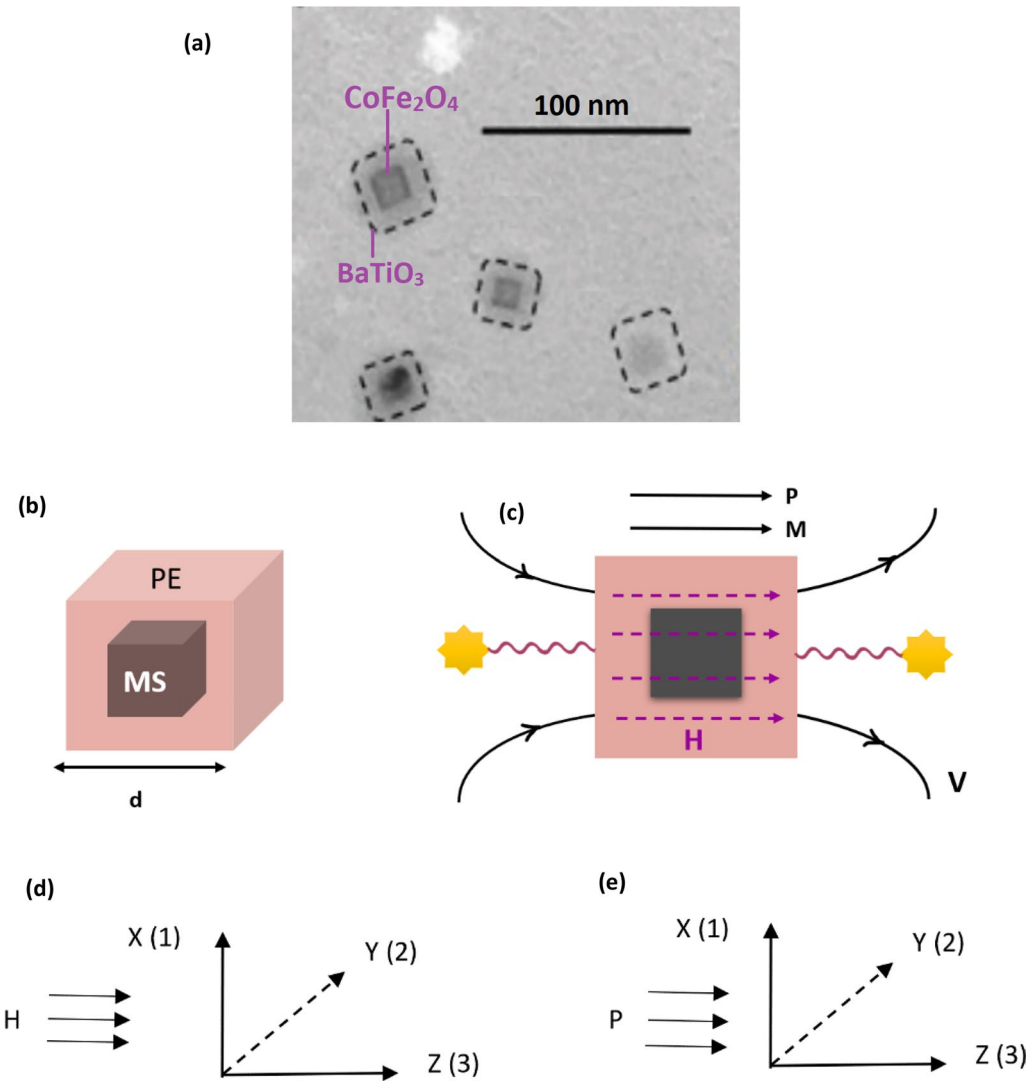

Fig. 3 (a) $CoFe_2O_4/BaTiO_3$ composite nanoparticle samples; transmission electron microscopy (TEM) image of cube-shaped MENPs, (b) A nanocomposite heterostructure, in which the (c) ME effect originates at the interface of lattice matched PE and MS component; *P* and *M* are the polarization and magnetization of the nanoparticles, respectively, *d* is the length of the composite nanoparticle, (d) local coordinate in the MS layer, and (e) local coordinate in the PE layer.

studied core–shell structures are made of the MS spinel core $CoFe_2O_4$ (ferrimagnetic) with an area of A_1 and the PE perovskite shell $BaTiO_3$ (ferroelectric) with an area of A_2. The length of the nanoparticle is d, while P and M are the polarization and magnetization of the nanoparticles, respectively (Fig. 3b). The nanoparticles can be conjugated with a load, e.g., a bio-load such as Paclitaxel. As explained below in Section "Dynamic Formalism", the bio-load can be conjugated with different techniques.[44–48]

MS deformation occurs predominantly along the sample's maximal dimension for any given set of geometric dimensions (Fig. 3b). In Fig. 3c, the local coordinate of the MS layer is $Z(3)$, therefore application of an AC magnetic field, H_{ac}, across the thickness would alternatively stretch and shrink the MS along the main strain direction. Because of the longitudinal polarization of the PE layer, it is subjected to a change along the same direction, which results in generation of a voltage across the thickness (designated as $Z(3)$ in the local coordinate system of the PE layer in Fig. 3d). The PE layer is forced to vibrate along the longitudinal direction as a result of stress coupling, which results in the induction of a voltage between the electrode ends (assuming that the applied H_{ac} is sinusoidal and that the associated vibrational motion of the nanoparticle composite along the longitudinal or $\hat{z}$ axis is similarly sinusoidal (harmonic motion). Magnetostriction causes shape changes in the ferrite particles in a PE perovskite and spinel-structure phase composite, and this strain is subsequently passed to the PE particles, resulting in electrical polarization. For comparison, the ME effect that is produced by this is 100 times stronger than the effect produced by the single-phase ME material, Co_2O_3.[11]

Neither the ferroelectric phase nor the ferrimagnetic phase possesses a significant ME effect; nonetheless, composites of these two phases exhibit a notable ME effect due to the strain-induced lattice-matched interface coupling between MS and PE components. The ME effect is therefore a combination of the MS effect (magnetic–mechanical effect) in the ferrimagnetic phase and the PE effect (mechanical–electrical effect) in the ferroelectric phase. The mechanical strain is linked to the magnetic and electric fields in the MS and PE components, respectively, thus leading to a pseudo-ME effect. Hence, the pseudo-ME effect due to the strain-coupled magnetic and electric components can be phenomenologically described according to[11,49:]

$$\text{Magnetoelectric effect} = \frac{\text{Mechanical}}{\text{Magnetic}} \times \frac{\text{Electric}}{\text{Mechanical}} \tag{2}$$

The ME coefficient is the most significant physical characteristic for MENPs. Therefore, its frequency dependence is vital for most applications.

Equivalent Circuit model of Magnetoelectric Nanoparticles

Based on the previous part, when a magnetic field is applied to a MENP, the MS part can be modeled as a receiver/oscillator, and the MS/PE coupling can be modeled as a transformer. In the rest of this study, we study the extraction of the related parameters to have a circuit model of MENPs.

Figure 4 shows the derived magneto-elasto-electric equivalent circuit for multiferroic and magnetoelectric composite nanoparticles. In this case, the coupling factor ϕ_m transforms the external magnetic field (H) into a mechanical voltage ($\phi_m H$). A transformer, ϕ_p , can be used to represent the electromechanical coupling in the circuit. I_1 and I_2 are mechanical and electric currents, respectively, and H and V are the applied magnetic field and induced voltage, respectively. ϕ_m and ϕ_p are magneto-elastic coupling and elastic-electric coupling, respectively. The ME voltage coefficient, or the ratio of an induced electric field to an applied magnetic field, is an important parameter for the direct-ME. According to this equivalent circuit and based on transformer and Kirchhoff's voltage and current laws, the ME voltage coefficient, $\alpha_E(\omega)$ as a function of the AC magnetic field frequency, can be obtained as:

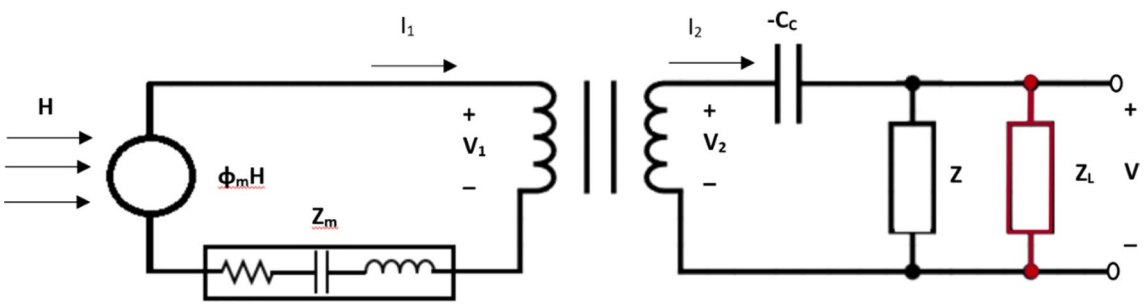

Fig. 4 Magnetoelectric equivalent circuit with added bioload as an impedance.

$$\frac{V_1}{V_2} = \phi_{\mathrm{p}}, \frac{I_1}{I_2} = \frac{1}{\phi_p} \tag{3}$$

$$V_1 = \phi_{\mathrm{m}} H - Z_{\mathrm{M}} I_1 \tag{4}$$

$$\frac{V_1}{V_2} = \frac{\phi_{\mathrm{m}} H - Z_{\mathrm{M}}\left(\frac{V}{(Z_{\mathrm{L}}||Z)\phi_{\mathrm{p}}}\right)}{\left(\frac{(Z_{\mathrm{L}}||Z)+C_{\mathrm{c}}}{Z_{\mathrm{L}}||Z}\right)V} = \phi_{\mathrm{p}} \tag{5}$$

$$V = \frac{\phi_{\mathrm{m}} H}{\left(\frac{(Z_{\mathrm{L}}||Z)+C_{\mathrm{c}}}{Z_{\mathrm{L}}||Z}\right)\phi_{\mathrm{p}} + \left(\frac{Z_{\mathrm{M}}}{(Z_{\mathrm{L}}||Z)\phi_{\mathrm{p}}}\right)} \tag{6}$$

$$\alpha_{\mathrm{E}}(\omega) = \frac{\partial V}{\partial H} = \frac{\phi_{\mathrm{m}}}{\left(\frac{(Z_{\mathrm{L}}||Z)+C_{\mathrm{c}}}{Z_{\mathrm{L}}||Z}\right)\phi_{\mathrm{p}} + \left(\frac{Z_{\mathrm{M}}}{(Z_{\mathrm{L}}||Z)\phi_{\mathrm{p}}}\right)} \tag{7}$$

where Z_{m} and Z_{L} are the motional and bio-load impedances, respectively, C_{c} is the clamped capacitance of the PE material, ∂H is the amount of change in the external magnetic field, and ∂V is the incremental electric field due to the change in the external magnetic field. To find the ME voltage coefficient, it is necessary to determine the magnetic-elastic factor (ϕ_{m}), the PE coupling factor (ϕ_{p}), Z_{m}, C_{c}, Z, and Z_{L}.

Magnetic-Elastic Factor (ϕ_{m})

An applied magnetic field, H, acts as a mechanical voltage, $\phi_{\mathrm{m}} H$, via a coupling factor, ϕ_{m}. The ME coupling factor, ϕ_{m}, can be thought of as a model for the MS transduction:

$$\phi_{\mathrm{m}} = \frac{A_1 d_{33,\,\mathrm{m}}}{s_{33}^{H}}\left[\frac{\mathrm{N}}{\frac{\mathrm{A}}{\mathrm{m}}}\right] \tag{8}$$

The total area of the MS layers' cross-section is denoted by A_1. ${S_{33}}^{H}$ is the elastic compliance of the MS material in longitudinal direction, which is the ratio of the relative deformation, S, to the mechanical stress, T (s^H is the compliance under a constant magnetic field). $d_{33,\mathrm{m}}$ is the piezomagnetic coefficient in longitudinal direction, which is defined by $d\lambda/dH$, and λ is the magnetostriction of a given MS material. It is worth mentioning that the 33 (stock configuration) mode and the 31 (bender configuration) mode are the two primary functioning modes in PE materials. In most cases, the PE charge constant, d_{33}, values of the 33 mode are greater than those of the other modes.[50]

Piezoelectric Coupling Factor (ϕ_{p})

The PE transduction is modeled by the PE coupling factor (ϕ_{p}):

$$\phi_{\mathrm{P}} = \frac{wlg_{33,\mathrm{p}}}{th_{\mathrm{p}} s_{33}^{D} \overline{\beta}_{33}^{T}}\left[\frac{\mathrm{N}}{\mathrm{V}}\right] \tag{9}$$

where w and l are the width and length of a nanoparticle (core–shell composite nanoparticle), respectively, th_p is the thickness of the PE material, ${s_{33}}^{D}$ is the longitudinal compliance (s^D is the compliance under a constant electric displacement), $\overline{\beta}_{33}^{T}$ is the inverse dielectric constant, and $g_{33,}$ is the longitudinal PE voltage coefficient. The voltage output constant, or PE voltage coefficient, is the ratio of the electric field generated to the mechanical stress applied, and is measured in the unit of voltage meter/Newton (Vm/N). It is calculated from the PE charge (strain) constant, d', and relative permittivity, ε, as $g = d'/\varepsilon$ (Vm/N).

Clamped Capacitance of the Piezoelectric Material (C_{c})

The capacitance in the circuit (capacitance of dielectric, C_{c}), is the clamped capacitance of the PE material. Its value can be obtained with the sample being fully constrained from motion during measurement:

$$C = \frac{\overline{\varepsilon}_{33} A}{d} \tag{10}$$

$$C_{\mathrm{c}} = \frac{A_2}{th_{\mathrm{p}} \overline{\beta}_{33}^{T}}\left[\frac{\mathrm{N}}{\mathrm{V}}\right] \tag{11}$$

The value for $\overline{\beta}_{33}^{T}$ is calculated by:

$$\overline{\beta}_{33}^{T} = \beta_{33}^{T}\left(1 + \frac{g_{33,\mathrm{p}}^2}{s_{33}^{D}\beta_{33}^{T}}\right)\left[\frac{\mathrm{m}}{\mathrm{F}}\right] \tag{12}$$

C_{c} is a negative parameter. The stored energy of a phase leads to a negative capacitance in ferroelectric materials. In Ref. [51], a theoretical study demonstrated how negative capacitance in nanodomains of a ferroelectric thin film can be stabilized. When elastic and electrostatic energy compete, the polarization in the $BaTiO_3$ layer forms arrays of clockwise and anticlockwise vortex-like structures to balance the system. In the core of these vortices, there are areas with suppressed polarization and more energy density, where the change in the internal field is bigger than the change in the external field. This makes the curvature of $\partial^2 G/\partial D^2$ negative (G = free energy). Negative capacitance areas are found to have higher energy density and larger polarizability, and are

thus the domain walls where the polarization is suppressed, as determined by a simultaneous vector mapping of atomic displacements (related to a complex pattern in the polarization field) and a reconstruction of the local electric field.[52] In other words, even in the locations where the permittivity itself is negative, the local susceptibility is always positive. When the susceptibility is very high, the material is highly polarizable and negative permittivity regions form. Negative capacitance appears in locations where polarization is repressed, a phenomenon made possible by the formation of domain walls, which in turn are made possible by vortices. As a result of the presence of vortices, negative capacitance arises.

Linear Constitutive Equations

The nanoparticle composite used in this model has two layers and is cubic in shape; it is made of $BaTiO_3$@$CoFe_2O_4$. As a result of the stress–strain interaction, the composite's layers are bound together. By following the electromechanical and magneto-elastic equivalent circuit techniques for laminates,[53] our theory can start with two sets of linear constitutive equations that are linked to each other.

Magnetostrictive Constitutive Equations

Strain, S_3 , is excited along the length of the nanoparticle composite when a H_{ac} is applied parallel to the $\hat{z}$ axis. Constitutive equations for S_3 and the magnetic field flux density, B_3 , in the MS regime are:

$$S_{3m} = S_{33}^{H} T_{3m} + d_{33,m} H_3 \tag{13}$$

$$B_3 = d_{33,m} T_{3m} + \mu_{33}^{T} H_3 \tag{14}$$

where H_3 is the magnetic field along $\hat{z}$, S_{3m} and T_{3m} are the strain and stress in the MS layers along $\hat{z}$, $s^{H}{}_{33}$, $d_{33,m}$, and $\mu^{T}{}_{33}$ are the elastic compliance at constant H, the longitudinal piezomagnetic constant, and the magnetic permeability at constant stress in the MS layers, respectively.

Piezoelectric Constitutive Equations

The PE is poled along its length, or $\hat{z}$ direction, in:

$$S_{3p} = S_{33}^{D} T_{3p} + g_{33,p} D_3 \tag{15}$$

$$E_3 = -g_{33,p} T_{3p} + \beta_{33}^{T} D_3 \tag{16}$$

$$E_3 = -g_{33,p} \frac{S_{3p}}{S_{33}^{D}} + \left[\beta_{33}^{T} \left(1 + \frac{g_{33,p}^2}{S_{33}^{D} \beta_{33}^{T}} \right) \right] D_3 = -g_{33,p} \frac{S_{3p}}{S_{33}^{D}} + \overline{\beta}_{33}^{T} D_3 \tag{17}$$

Integrating along the length d of the nanoparticle composite along the z axis, the coupling voltage, V, produced at the two electrode surfaces of the PE induced by MS layer can be calculated as:

$$V = \int_0^d E_3 dz = -\frac{g_{33,p}}{jw} \frac{1}{S_{33}^{D}} \left(\dot{u}_2 - \dot{u}_1 \right) + \overline{\beta}_{33}^{T} D_3 d \tag{18}$$

where $D_3$and E_3 denote the dielectric displacement and electric field in the z-direction of the PE layer, respectively, the strain and stress in the PE layer along $\hat{z}$ are denoted by S_{3p} and T_{3p}, respectively, and d is the length of the composite nanoparticle.

Correspondingly, the coupling current I_2 produced by the PE layer is:

$$I_2 = \frac{dQ}{dt} = \frac{A_2 dD_3}{dt} = j\omega Q \tag{19}$$

$$Q = \int_0^l \int_0^w D_3 dx dz \tag{20}$$

The Electrical Impedance in the Circuit (Z)

Parameter Z in our proposed equivalent circuit model represents the electrical impedance in the circuit, reflecting the contribution of the clamp effect. In the absence of any bioload (in an open circuit), I_2 from the PE part is zero; thus, the loads (Z and $-C_0$) can be moved into the main circuit loop. Applying Ohm's law to the equivalent circuit of Fig. 4, the electrical impedance in the circuit, Z, can be calculated using:

$$Z = \frac{V}{I_2} \tag{21}$$

$$V = \int_0^d E_3 dz \tag{22}$$

$$Z = \frac{-\frac{g_{33,p}}{jw} \frac{1}{S_{33}^{D}} \left(\dot{u}_2 - \dot{u}_1 \right) + \left[\beta_{33}^{T} \left(1 + \frac{g_{33,p}^2}{S_{33}^{D}} \right) \right] D_3 d}{\frac{A_2 dD_3}{dt}} \tag{23}$$

Bioload Impedance (Z_L)

So far, an equation for the ME coefficient has been developed for MENPs in the absence of a bioload. To consider Z_L in the circuit, we need to know the nature of the MENPs' surface coating. Different types of organic materials can be used to coat the surface of an inorganic core–shell nanostructure.[54] Figure 5 shows that different

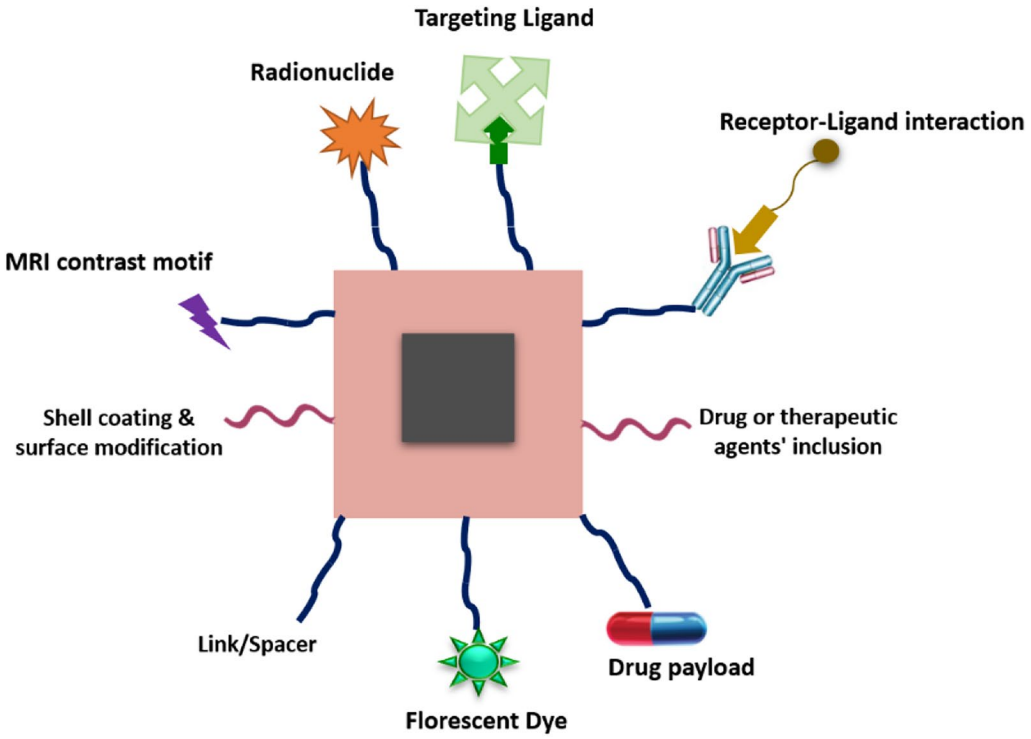

Fig. 5 Different bioloads that can be attached to the MENPs.

modification protocols can be used to add different functionalities, targeting ligands, imaging probes, and therapeutic payloads to the nanoparticles. However, not every possible modification is necessary for a single nanoparticle. Specifically defined therapeutic goals will lead to the necessary strategies for structure design and functionalization, which will lead to the best performance in real-world medical applications.[2] Functionalization refers to the surface modification of nanoparticles through conjugation of functional groups and/or biomolecules to improve targeting efficiency.

Because each method has its own set of inherent benefits and drawbacks, it can be very difficult for researchers to choose the conjugation technique that would be most effective. For instance, nanoparticles can be functionalized with antibodies or antibody fragments through the use of three different surface modification methods: (1) adsorption, which is a non-covalent immobilization strategy that includes physical adsorption[44] and ionic binding;[45,46] (2) covalent strategies[47] consisting of carbodiimide chemistry,[55,56] maleimide chemistry[57] and click-chemistry;[58] and (3) binding by adapter molecules[48] like biotin–avidin system.[59]

In an ideal scenario, the conjugation procedure should offer site-specificity, correct spatial orientation, adequate loading density onto the nanoparticle, and preserved antigen binding activity. In spite of the significant amount of work that has been put into the field of bioconjugation, there is no one method that possesses all of these features to be considered best; however, click chemistry[57] has shown that it indeed satisfies the majority of the criteria.

Therefore, researchers anticipate that this strategy will be at the forefront of conjugation for therapeutic applications or, at the very least, become a valuable conjugation platform in the same way that it is for biomedical applications such as diagnosis and imaging.[60–62] In addition, when immobilizing antibodies, conjugation should be used to ensure that the correct orientation and the desired amount of these biomolecules (density) are packed into each nanoparticle. Because of this, each has its own unique impedance.

In the case of MENPs, the research literature includes reports of numerous techniques for stabilization that involve coating the surface with a layer of polymer. For example, in early studies, poly(L-lysine) or polyethylene glycol (PEG) was used to create $BaTiO_3$ nanoparticle (BTNP) dispersions that were stable for multiple days.[30] These dispersions were created by wrapping the nanoparticle surface. On the other hand, it was discovered that the polymer could cause cytotoxic effects. Since that time, it has been possible to create BTNP dispersions that are stable and free of cytotoxic effects by using other polymers such as glycol chitosan (GC) or polyethyleneimine. It is one of the earliest cationic polymers to be used for gene delivery, including the delivery of RNA,

and it has been the subject of most research.[63] The current methods of polymeric wrapping rely on nonspecific adsorption and noncovalent binding, both of which have the potential to reduce the stability of the polymers in biological environments. GC, a water-soluble chitosan derivative with hydrophilic ethylene glycol branches, possesses both hydrophobic segments that are useful for the encapsulation of a variety of drugs and reactive functional groups that make it simple to make chemical modifications. Reference [64] provides an overview of the recent developments of GC-based materials in the areas of cell surface labeling, multimodal tumor imaging, and the encapsulation and delivery of drugs (chemotherapeutics, photosensitizers, nucleic acids, and antimicrobial agents) for the treatment of cancers and microbial infections. Cyclodextrin (CD)-stabilized $BaTiO_3$ nanoparticles were made by first hydroxylating the nanoparticle surface and then covalently attaching CD molecules. This made stable and noncytotoxic dispersions of $BaTiO_3$ nanoparticles.[65]

Traditional solid-state methods produce $BaTiO_3$ nanoparticles with broad size distributions and poor aqueous dispersibility. Ciofani et al. demonstrated cytocompatibility of $BaTiO_3$ nanoparticles non-covalently stabilized by GC at concentrations up to 100 g/mL.[66] Pantazis and colleagues introduced $BaTiO_3$ nanoparticles as second harmonic generation nanoprobes for in vivo imaging in living zebrafish embryos.[67] Luke and coworkers reported a method for producing antibody-conjugated $BaTiO_3$ nanoparticles which exhibit cell-specific targeting ability.[68] The gel collection method for BTNP synthesis was disclosed by Huang and colleagues,[69] along with three methods for surface modification. For the production of $BaTiO_3$@Citrate nanoparticles, molecular adsorption is used, but there are also other methods, such as silica coating via the Stöber process and silica coating via reverse microemulsion.

Researchers have investigated a strategy for modifying the surfaces of $BaTiO_3$ nanoparticles by first hydroxylating them and then covalently attaching hydrophilic PEG polymers in Ref. [68]. Among various polymers, synthetic PEG has traditionally been regarded as the gold standard for enabling inorganic nanoparticle biomedical applications.[54] Additional modifications, such as fluorescent labeling, surface charge tuning, or directional conjugation of IgG antibodies, are possible with this polymer coating. They demonstrated anti-EGFR antibody conjugation to the $BaTiO_3$ nanoparticles surface, as well as efficient molecular targeting of the nanoparticles to A431 cells. Overall, the reported modifications aim to broaden the applications of $BaTiO_3$ nanoparticles in molecular imaging, cancer therapy, and noninvasive neurostimulation. In our case, we used $BatiO_3$ with a PEG coating.

Different therapeutic goals necessitate distinct structural design and functionalization methodologies, with optimal performance achieved by targeting nanoparticles to certain anatomical locations within the body. As a result, the bioload impedance is conditional on a variety of factors, and it is important to understand where exactly the load will land in the body and how it is going to bind.[15] In our subsequent investigation, we intend to study the impedance variations depending on all these conditions.

Dynamic Formalism

By solving the second-order equation of motion for the system, the remaining mechanical parameters can be determined. The MS and PE constitutive equations have previously been integrated in analyses of MS/PE laminates.[70] However, this does not provide a sufficient understanding of the energy coupling that occurs between layers under dynamic settings. Coupling, as determined by an equation of motion, is necessary for thorough analysis. Assume that the vibrational motion of the nanoparticle composite is sinusoidal (harmonic motion) along the longitudinal or z axis, and that a sinusoidally applied H_{ac} causes this motion. This will allow us to determine how the nanoparticle composite will behave. The PE mass units (Δm_1) and the MS mass units (Δm_2) found in the nanoparticle composite have identical displacement $u(z)$ and strain $\partial u/\partial z$ components along $\hat{}z$, which may be expressed as:

$$u_{3p} = u_{3m} = u(z) \tag{24}$$

H_{ac} is applied parallel to the longitudinal vibration direction and number 3 means both are in z direction.

$$S_{3p} = S_{3m} = \frac{\partial u}{\partial z} \tag{25}$$

$$\frac{\partial S_{3p}}{\partial z} = \frac{\partial S_{3p}}{\partial t}\frac{\partial t}{\partial z} \tag{26}$$

The nanoparticle composite has an equation of motion that is consistent with Newton's second law, which is:

$$F = ma = \left(\Delta m_1 + \Delta m_2\right)\frac{\partial^2 u}{\partial t^2} \tag{27}$$

$$\Delta T_{3m}A_1 + \Delta T_{3p}A_2 = \left(\Delta m_1 + \Delta m_2\right)\frac{\partial^2 u}{\partial t^2} \tag{28}$$

where $\Delta m_1 = \rho_{ms}A_1\Delta z$, $\Delta m_2 = \rho_{pe}A_2\Delta z$, ρ_{pe} and ρ_{ms} are the mass densities of the PE and MS layers, and A_1 and A_2 cross-sectional area of the MS and PE layers, respectively. MENP's cross-sectional area for a given width, w, is $A = A_1 + A_2 = t_{composite}w$. $A_1 = t_{ms}w$; $A_2 = t_{pe}w$; t_{pe} and t_{ms} are the

thicknesses of the PE and MS layers; $t_{composite}$ is the total thickness of the nanoparticle composite.

The equation of motion can be re-written as:

$$\begin{aligned}\left(\Delta m_1 + \Delta m_2\right)\frac{\partial^2 u}{\partial t^2} &= \Delta T_{3m}A_1 + \Delta T_{3p}A_2 \\ &\rightarrow \left(\rho_{ms}A_1\Delta z + \rho_{pe}A_2\Delta z\right)\frac{\partial^2 u}{\partial t^2} \\ &= \Delta T_{3m}A_1 + \Delta T_{3p}A_2\end{aligned} \tag{29}$$

$$\left(\rho_{ms}A_1 + \rho_{pe}A_2\right)\frac{\partial^2 u}{\partial t^2} = \frac{\Delta T_{3m}A_1 + \Delta T_{3p}A_2}{\Delta z} \tag{30}$$

$$\frac{\left(\rho_{ms}A_1 + \rho_{pe}A_2\right)}{A}\frac{\partial^2 u}{\partial t^2} = \frac{\Delta T_{3m}}{\Delta z}\frac{A_1}{A} + \frac{\Delta T_{3p}}{\Delta z}\frac{A_2}{A} \tag{31}$$

$$\rho_{aveg} = \frac{\rho_{ms}A_1 + \rho_{pe}A_2}{A}\left[\mathrm{kg/m^3}\right] \tag{32}$$

$$\frac{A_1}{A} = n, \frac{A_2}{A} = (1-n), 0 \prec n \prec 1 \tag{33}$$

$$\rho_{aveg}\frac{\partial^2 u}{\partial t^2} = n\frac{\partial T_{3m}}{\partial z} + (1-n)\frac{\partial T_{3p}}{\partial z} \tag{34}$$

where ρ_{aveg} is the average mass density of the nanoparticle composite.

The sound velocity (υ) of the nanoparticle composite can be related to the equation of motion if either Eqs. (13) or (15) are substituted into (34), and if the definition of strain given in (24) is used. The resulting equations are:

$$\frac{\partial^2 u}{\partial t^2} = v^2\frac{\partial^2 u}{\partial z^2} \tag{35}$$

$$v^2 = \left(\frac{n}{S_{33}^H} + \frac{(1-n)}{S_{33}^D}\right)/\rho_{aveg}, \left[\left(\frac{\mathrm{m}}{\mathrm{s}}\right)^2\right] \tag{36}$$

Under harmonic oscillation, (33) then becomes:

$$\frac{\partial^2 u}{\partial z^2} = \frac{1}{v^2}\frac{\partial^2 u}{\partial t^2} \tag{37}$$

$$\frac{\partial^2 u}{\partial z^2} + k^2 u = 0, k^2 = \left(\frac{\omega}{v}\right)^2 \tag{38}$$

where k and ω are the wave number and the angular frequency, respectively.

Mechanical Impedance (Z_m)

The electrical analogues of the parameter, Z_m , derived from the motion/constitutive equations is:

$$Z_m = -\frac{1}{2}j\rho_{ave}\upsilon\left(A_1 + A_2\right)\cot\frac{kd}{2} \tag{39}$$

$$\alpha_E(\omega) = \frac{A_1 d_{33,m}}{s_{33}^H\left(1 + \left(\frac{A_2}{th_p\bar{\beta}_{33}^T}\right)^2\frac{g_{33p}}{Zs_{33}^D}\right) - j\left(\frac{\rho_{ave}\upsilon A th_p s_{33}^D\bar{\beta}_{33}^T s_{33}^H}{2(Z)w\lg_{33p}}\cot\frac{kl}{2}\right)} \tag{40}$$

where Z_m consists of R_m, C_m, and L_m which are motional resistance, inductance, and capacitance of the nanoparticle, respectively ($Z_m = R_m + j(\omega L_m + (1/\omega C_m))$. At a resonance frequency of $\omega_s = (1/L_m C_m)^{½}$. Therefore, Eq. (40) can be written at a resonance frequency (ω_r) in which the $\alpha_E(\omega)$ reaches a maximum value. According to this equivalent circuit, this frequency is determined by the nanoparticles' parameters:

$$\begin{aligned}\alpha_E(\omega_r) &= \frac{\phi_m}{\left(1 + \frac{C_c}{Z}\right)\phi_p + \left(\frac{R_m}{(Z)\phi_p}\right)} \\ &= \frac{A_1 d_{33,m}}{s_{33}^H\left(1 + \left(\frac{A_2}{th_p\bar{\beta}_{33}^T}\right)^2\frac{g_{33p}}{Zs_{33}^D}\right) + \left(\frac{R_m th_p s_{33}^D\bar{\beta}_{33}^T s_{33}^H}{(Z)wlg_{33p}}\right)}\end{aligned} \tag{41}$$

Finally, the MENP magnetoelectric voltage coefficient without any bioload can be written as Eq. (41). The $CoFe_2O_4$@$BaTiO_3$ composite nanoparticles can have a ME coefficient on the order of 5 V cm^{-1} Oe^{-1} to 10 V cm^{-1} Oe^{-1} at a resonance frequency.[12] A magnetic field of 1000 Oe would create an electric field of 10,000 V/cm (= 1 mV/nm) upon application.[71] Basic "back-of-the-envelope" physics calculations suggest that the ME coefficient could be above 10 V cm^{-1} Oe^{-1} for a lattice-matched interface, if the core's magnetostriction constant is −200 ppm and the shell's PE constant is ~190 pC/N.[12,72]

Figure 6 shows the ME voltage coefficient versus frequency for MENPs. The resonance frequency of nanoparticles is influenced by various factors, including their size, shape, composition, and the interaction between different materials within the composite.[73] Typically, mechanical resonance frequencies in the GHz range can be observed in nanoparticles with dimensions in the order of nanometers.[74] In the case of $CoFe_2O_4$/$BaTiO_3$ core–shell MENPs, the specific nanoparticle size distribution and composition will play a crucial role in determining the resonance frequency. Smaller nanoparticles tend to exhibit higher resonance frequencies because of their mechanical vibrations. Considering the nanoparticle size on the order of 30 nm, it

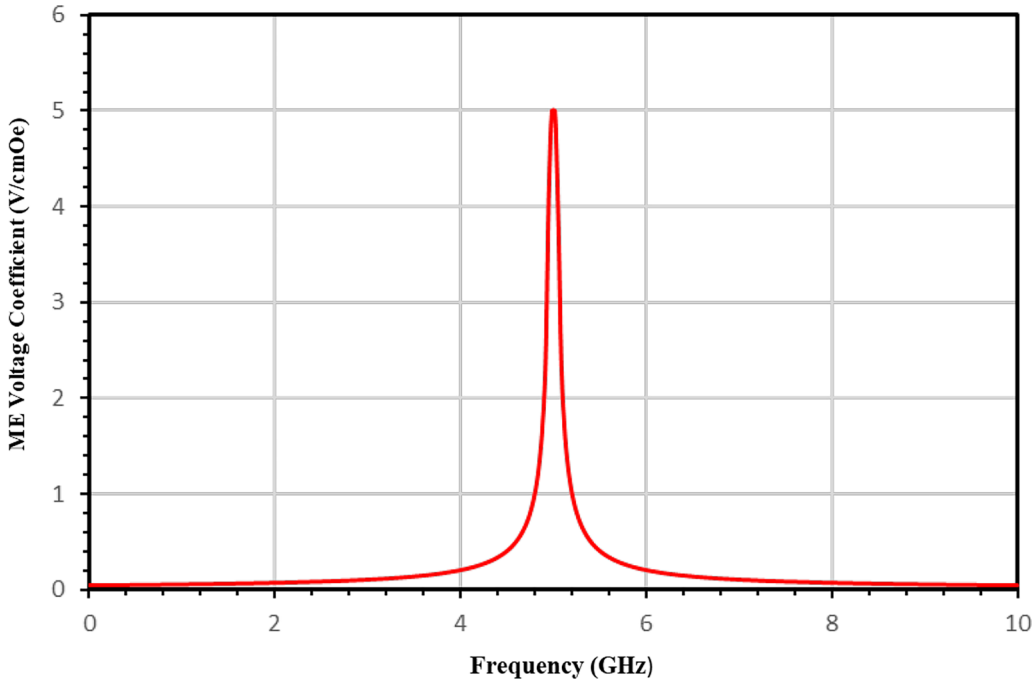

Fig. 6 ME voltage coefficient versus frequency for MENPs.

Table I Parameters for extracting voltage coefficient versus frequency

Symbol	Definition	Value
L_c	Core length	20 nm
L_s	Shell length	10 nm
$d_{33,m}$	The magneto-elastic or piezomagnetic coefficient in longitude direction	~ 200 pC/N
w	Width of a nanoparticle (core–shell composite nanoparticle)	30 nm
l	Length of a nanoparticle (core–shell composite nanoparticle)	30 nm
th_p	The thickness of the PE	10 nm
$S_{33}{}^H$	The elastic compliance of the MS material in longitude direction	~17.3×10^{-12} m^2/N
$g_{33,p}$	The longitude PE voltage coefficient	~ 44.2 pC/N to 44.8 pC/N
S_{3m}	The stress in the MS layers along $z\hat{}$	~−10 × 109 dyne/cm^2
T_{3p}	Stress in the PE layer along $\hat{}z$	~−20×109 dyne/cm^2
μT_{33}	The magnetic permeability at constant stress in the MS layers	100×10^{-6} Ns2/C2
λ	The magnetostriction of MS material ($CoFe_2O_4$)	−200 ppm
ρ_{pe}	Mass densities of the PE layer ($BaTiO_3$)	~6 g/cm^3

is reasonable to expect that the resonance frequency would fall towards the higher end of the range, possibly around 5–10 GHz.[12] It can be noted that the current model does not take into account intrinsic materials resonance such as ferromagnetic or ferroelectric resonances, which do not depend on the size.[75,76] In the next study, we would like to incorporate these effects in dynamic calculations.

Parameters for extracting voltage coefficient versus frequency are listed in Table I. It is important to note that, like any modeling study, there may be simplifications and assumptions made in the development of the equations and the equivalent circuit model. These simplifications might overlook certain complex factors that could influence the behavior of magnetoelectric nanoparticles in real-world scenarios.

Conclusions

This study has introduced novel equivalent circuits to derive phenomenological expressions capable of capturing the frequency dependence of the magnetoelectric coefficient

in MENPs in biological microenvironments. Specifically, the investigations focused on the widely used $CoFe_2O_4$@$BaTiO_3$ two-phase core–shell configuration. The obtained resonance frequency in the gigahertz range is in agreement with available experimental measurements according to literature. Importantly, these derivations can be readily extended to encompass other core–shell nanoparticles, as well as various composite and even single-phase multiferroic nanostructures.

The developed magneto-elasto-electric effect equivalent circuit integrates MS and PE constitutive equations, along with an equation of motion to accommodate dynamic effects. Additionally, this circuit model has also optionally considered the bio-loads conjugated to the nanoparticles. Through longitudinal data analysis of cube-shaped MENPs, the model offers insights into the MENPs' characteristics under different conditions. Looking ahead, there is potential for further refinement and expansion of this model. Future studies could incorporate intrinsic composition-specific resonances, such as the ferromagnetic resonance in the MS component and the ferroelectric resonance in the PE component. This equivalent circuit model can deepen the general understanding of fundamental biological processes that may be intelligently and wirelessly controlled using MENPs, leveraging specific spatiotemporal patterns of magnetic and electric fields. Overall, this study contributes to the ongoing exploration of MENPs and their potential applications in biomedical contexts. The development of robust equivalent circuit models lays the foundation for future investigations and paves the way for innovative approaches to control and manipulate biological systems with unprecedented precision.

Funding This research was partially supported by the Defense Advanced Research Projects Agency (DARPA) and Naval Information Warfare Center, Pacific (NIWC Pacific) under Contract N66001-19-C-4019 or N6600119C4019. The study was also partially supported by the National Science Foundation (NSF) under award #ECCS-211082.

Conflict of interest The authors declare that they have no conflict of interest.

References

1. P. Gehr and R. Zellner, *Biological Responses to Nanoscale Particles* (Cham: Springer, 2019).
2. Z. Liu, F. Kiessling, and J. Gätjens, Advanced nanomaterials in multimodal imaging: design, functionalization, and biomedical applications. *J. Nanomater.* 2010, 894303 (2010).
3. S. Khizroev and P. Liang, Engineering future medicines with magnetoelectric nanoparticles: wirelessly controlled, targeted therapies. *IEEE Nanotechnol. Mag.* 14(1), 23 (2020). https://doi.org/10.1109/Mnano.2019.2952227.
4. K. Yue, R. Guduru, J.M. Hong, P. Liang, M. Nair, and S. Khizroev, Magneto-electric nano-particles for non-invasive brain stimulation. *PLoS ONE* 7(9), e44040 (2012). https://doi.org/10.1371/journal.pone.0044040.
5. E.H. Apu, M. Nafiujjaman, S. Sandeep, A.V. Makela, A. Khaleghi, S. Vainio, C.H. Contag, J. Li, I. Balasingham, T. Kim, and N. Ashammakhi, Biomedical applications of multifunctional magnetoelectric nanoparticles. *Mater. Chem. Front.* 6(11), 1368 (2022).
6. R.J. DeBerardinis and N.S. Chandel, Fundamentals of cancer metabolism. *Sci. Adv.* 2(5), e1600200 (2016).
7. M. Levin, Bioelectric mechanisms in regeneration: unique aspects and future perspectives. *Semin. Cell Dev. Biol.* 20(5), 543 (2009).
8. C. Chen, X. Bai, Y. Ding, and I.-S. Lee, Electrical stimulation as a novel tool for regulating cell behavior in tissue engineering. *Biomater. Res.* 23, 1 (2019).
9. L. Mitoseriu, Magnetoelectric phenomena in single-phase and composite systems. *Bol. Soc. Esp. Cerám. Vidr.* 44(3), 177 (2005).
10. S. Ahmed, M. Atif, A. Ur Rehman, S. Bashir, N. Iqbal, W. Khalid, Z. Ali, and M. Nadeem, Enhancement in the magnetoelectric and energy storage properties of core–shell-like $CoFe_2O_4$-$BaTiO_3$ multiferroic nanocomposite. *J. Alloys Compd.* 883, 160875 (2021).
11. C.-W. Nan, Magnetoelectric effect in composites of piezoelectric and piezomagnetic phases. *Phys. Rev. B* 50(9), 6082 (1994).
12. P. Wang, E. Zhang, D. Toledo, I. Takako-Smith, B. Navarrete, N. Furman, A. Franco-Hernandez, M. Telusma, D. McDaniel, P. Liang, and S. Khizroev, Colossal magnetoelectric effect in core–shell magnetoelectric nanoparticles. *Nano Lett.* 20(8), 5765 (2020).
13. K. Yue, R. Guduru, J. Hong, P. Liang, M. Nair, and S. Khizroev, Magneto-electric nano-particles for non-invasive brain stimulation. *PLoS ONE* 7(9), e44040 (2012). https://doi.org/10.1371/journal.pone.0044040.
14. E. Zhang, M. Abdel-Mottaleb, P. Liang, B. Navarrete, Y. Akin Yildirim, M. Alberteris Campos, I.T. Smith, P. Wang, B. Yildirim, L. Yang, S. Chen, I. Smith, G. Lur, T. Nguyen, X. Jin, B.R. Noga, P. Ganzer, and S. Khizroev, Magnetic-field-synchronized wireless modulation of neural activity by magnetoelectric nanoparticles. *Brain Stimul.* 15(6), 1451 (2022).
15. J. Jang and C.B. Park, Magnetoelectric dissociation of Alzheimer's β-amyloid aggregates. *Sci. Adv.* 8(19), 1675 (2022).
16. R. Guduru, P. Liang, C. Runowicz, M. Nair, V. Atluri, and S. Khizroev, Magneto-electric nanoparticles to enable field-controlled high-specificity drug delivery to eradicate ovarian cancer cells. *Sci. Rep.* 3(1), 1 (2013).
17. T.S. Stewart, A. Nagesetti, R. Guduru, P. Liang, E. Stimphil, A. Hadjikhani, L. Salgueiro, J. Horstmyer, R. Cai, A. Schally, and S. Khizroev, Magnetoelectric nanoparticles for delivery of antitumor peptides into glioblastoma cells by magnetic fields. *Nanomedicine* 13(4), 423 (2018).
18. B.J. Burkett, D.J. Bartlett, P.W. McGarrah, A.R. Lewis, D.R. Johnson, K. Berberoğlu, M.K. Pandey, A.T. Packard, T.R. Halfdanarson, C.B. Hruska, G.B. Johnson, and A.T. Kendi, A review of theranostics: perspectives on emerging approaches

and clinical advancements. *Radiol. Imaging Cancer* 5(4), e220157 (2023). https://doi.org/10.1148/rycan.220157.
19. A. Kaushik, J. Rodriguez, D. Rothen, V. Bhardwaj, R.D. Jayant, P. Pattany, B. Fuentes, H. Chand, N. Kolishetti, N. El-Hage, K. Khalili, N.S. Kenyon, and M. Nair, MRI-guided, noninvasive delivery of magneto-electric drug nanocarriers to the brain in a nonhuman primate. *Acs Appl. Bio Mater.* 2(11), 4826 (2019). https://doi.org/10.1021/acsabm.9b00592.
20. I. Bok, I. Haber, X.F. Qu, and A. Hai, In silico assessment of electrophysiological neuronal recordings mediated by magnetoelectric nanoparticles. *Sci. Rep.* 12(1), 8386 (2022). https://doi.org/10.1038/s41598-022-12303-4.
21. R. Guduru, P. Liang, M. Yousef, J. Horstmyer, and S. Khizroev, Mapping the brain's electric fields with magnetoelectric nanoparticles. *Bioelectron. Med.* 4(10), 1 (2018). https://doi.org/10.1186/s42234-018-0012-9.
22. P.L. Elric-Zhang, Y.A. Yildirim, S. Chen, M. Abdel-Mottaleb, M. Shotbolt, Z. Ramezani, J. Tian, V. Andre, and S. Khizroev, Ab initio physics considerations in the design of wireless and non-invasive neural recording systems using magnetoelectric nanoparticles. *IEEE Trans. Magn.* 59(10), 1 (2023). https://doi.org/10.1109/TMAG.2023.3300791.
23. A. Nagesetti, A. Rodzinski, E. Stimphil, T. Stewart, C. Khanal, P. Wang, R. Guduru, P. Liang, I. Agoulnik, J. Horstmyer, and S. Khizroev, Multiferroic coreshell magnetoelectric nanoparticles as NMR sensitive nanoprobes for cancer cell detection. *Sci. Rep.* 7, 14137 (2017). https://doi.org/10.1038/s41598-017-12311-9.
24. C. Navau, J. Prat-Camps, and A. Sanchez, Magnetic energy harvesting and concentration at a distance by transformation optics. *Phys. Rev. Lett.* 109(26), 263903 (2012).
25. S. Khizroev and P. Liang, Engineering future medicines with magnetoelectric nanoparticles: wirelessly controlled, targeted therapies. *IEEE Nanatechnol. Mag.* 14(1), 23 (2019).
26. A. Rodzinski, R. Guduru, P. Liang, A. Hadjikhani, T. Stewart, E. Stimphil, C. Runowicz, R. Cote, N. Altman, R. Datar, and S. Khizroev, Targeted and controlled anticancer drug delivery and release with magnetoelectric nanoparticles. *Sci. Rep.* 6, 20867 (2016). https://doi.org/10.1038/srep20867.
27. M. Nair, R. Guduru, P. Liang, J. Hong, V. Sagar, and S. Khizroev, Externally controlled on-demand release of anti-HIV drug using magneto-electric nanoparticles as carriers. *Nat. Commun.* 4, 1707 (2013). https://doi.org/10.1038/ncomms3729.
28. J.F. Gomes Marin, R.F. Nunes, A.M. Coutinho, E.C. Zaniboni, L.B. Costa, F.G. Barbosa, M.A. Queiroz, G.G. Cerri, and C.A. Buchpiguel, Theranostics in nuclear medicine: emerging and re-emerging integrated imaging and therapies in the era of precision oncology. *Radiographics* 40(6), 1715 (2020). https://doi.org/10.1148/rg.2020200021.
29. B.K. Kashyap, V.V. Singh, M.K. Solanki, A. Kumar, J. Ruokolainen, and K.K. Kesari, Smart nanomaterials in cancer theranostics: challenges and opportunities. *ACS Omega* 8(16), 14290 (2023). https://doi.org/10.1021/acsomega.2c07840.
30. E. Zhang, M. Abdel-Mottaleb, P. Liang, B. Navarrete, Y. Akin Yildirim, M. Alberteris Campos, I.T. Smith, P. Wang, B. Yildirim, L. Yang, S. Chen, I. Smith, G. Lur, T. Nguyen, X. Jin, B.R. Noga, P. Ganzer, and S. Khizroev, Magnetic- field-synchronized wireless modulation of neural activity by magnetoelectric nanoparticles. *Brain Stimul.* 15(6), 1451 (2022). https://doi.org/10.1016/j.brs.2022.10.004.
31. M. Liu and N.X. Sun, Voltage control of magnetism in multiferroic heterostructures. *Philoso. Trans. R. Soc. A Math. Phys. Eng. Sci.* 372(2009), 20120439 (2014).
32. A. Molinari, H. Hahn, and R. Kruk, Voltage-control of magnetism in all-solid-state and solid/liquid magnetoelectric composites. *Adv. Mater.* 31(26), 1806662 (2019).
33. R. Gao, Q. Zhang, Z. Xu, Z. Wang, W. Cai, G. Chen, X. Deng, X. Cao, X. Luo, and C. Fu, Strong magnetoelectric coupling effect in $BaTiO_3$@$CoFe_2O_4$ magnetoelectric multiferroic fluids. *Nanoscale* 10(25), 11750 (2018).
34. E. Hannachi and Y. Slimani, Advanced progress in magnetoelectric multiferroic composites: fundamentals, applications, and toxicity, *Handbook of Magnetic Hybrid Nanoalloys and their Nanocomposites*. (Cham: Springer, 2022), pp. 351–385.
35. W. Li, Z. Zhang, and D. Li, Rheological properties of silicon oil-based magnetic fluid with magnetic nanoparticles (MNPs)-multiwalled carbon nanotube (MWNT). *Smart Mater. Struct.* 28(6), 065023 (2019).
36. J. Zhang, H. Cui, S. Han, Z. Li, and J. Lu, Research on the rheological properties of a silicone oil-based ferrofluid. *Korea-Aust. Rheol. J.* 35(3), 179 (2023).
37. R. Gao, Q. Zhang, Z. Xu, Z. Wang, G. Chen, C. Fu, X. Deng, and W. Cai, Anomalous magnetoelectric coupling effect of $CoFe_2O_4$-$BaTiO_3$ binary mixed fluids. *ACS Appl. Electron. Mater.* 1(7), 1120 (2019).
38. A. Marrella, G. Suarato, S. Fiocchi, E. Chiaramello, M. Bonato, M. Parazzini, and P. Ravazzani, Magnetoelectric nanoparticles shape modulates their electrical output. *Front Bioeng. Biotechnol.* 11, 1219777 (2023). https://doi.org/10.3389/fbioe.2023.1219777.
39. K. Shahzad, S. Mushtaq, M. Rizwan, W. Khalid, M. Atif, F.U. Din, N. Ahmad, R. Abbasi, and Z. Ali, Field-controlled magnetoelectric core–shell $CoFe_2O_4$@$BaTiO_3$ nanoparticles as effective drug carriers and drug release *in vitro*. *Mater. Sci. Eng. C* 119, 111444 (2021).
40. E. Stimphil, A. Nagesetti, R. Guduru, T. Stewart, A. Rodzinski, P. Liang, and S. Khizroev, Physics considerations in targeted anticancer drug delivery by magnetoelectric nanoparticles. *Appl. Phys. Rev.* 4(2), 021101 (2017).
41. L.D. Landau, *Collected Papers of LD Landau* (Bergama: Pergamon, 1965).
42. M. Fiebig, Revival of the magnetoelectric effect. *J. Phys. D Appl. Phys.* 38(8), R123 (2005).
43. S. Khizroev, Technobiology's enabler: the magnetoelectric nanoparticle. *Cold Spring Harb. Perspect. Med.* 9(8), a034207 (2019).
44. M. Tallawi, E. Rosellini, N. Barbani, M.G. Cascone, R. Rai, G. Saint-Pierre, and A.R. Boccaccini, Strategies for the chemical and biological functionalization of scaffolds for cardiac tissue engineering: a review. *J. R. Soc. Interface* 12(108), 20150254 (2015).
45. S. Liebana and G.A. Drago, Bioconjugation and stabilisation of biomolecules in biosensors. *Essays Biochem.* 60(1), 59 (2016).
46. J. Goossens, H. Sein, S. Lu, M. Radwanska, S. Muyldermans, Y.G.-J. Sterckx, and S. Magez, Functionalization of gold nanoparticles with nanobodies through physical adsorption. *Anal. Methods* 9(23), 3430 (2017).
47. M.A. Parracino, B. Martín, and V. Grazú, State-of-the-art strategies for the biofunctionalization of photoactive inorganic nanoparticles for nanomedicine, *Photoactive Inorganic Nanoparticles*. (Amsterdam: Elsevier, 2019), pp. 211–257.
48. M.R. Gordon, M. Canakci, L. Li, J. Zhuang, B. Osborne, and S. Thayumanavan, Field guide to challenges and opportunities in antibody–drug conjugates for chemists. *Bioconjug. Chem.* 26(11), 2198 (2015).
49. A. Arnau and D. Soares, Fundamentals of piezoelectricity, *Piezoelectric Transducers and Applications*. (Cham: Springer, 2009), pp. 1–38.
50. N. Soin, S. Anand, and T. Shah, Energy harvesting and storage textiles, *Handbook of Technical Textiles*. (Amsterdam: Elsevier, 2016), pp. 357–396.
51. T. Sluka, P. Mokry, and N. Setter, Static negative capacitance of a ferroelectric nano-domain nucleus. *Appl. Phys. Lett.* 111(15), 152902 (2017).

52. A.K. Yadav, K.X. Nguyen, Z. Hong, P. García-Fernández, P. Aguado-Puente, C.T. Nelson, S. Das, B. Prasad, D. Kwon, S. Cheema, A.I. Khan, C. Hu, J. Íñiguez, J. Junquera, L.-Q. Chen, D.A. Muller, R. Ramesh, and S. Salahuddin, Spatially resolved steady-state negative capacitance. *Nature* 565(7740), 468 (2019).
53. M. Ruiz and A. Razzitte, Equivalent circuit model of magnetostrictive/piezoelectric laminate composite. *2016 IEEE Global Electromagnetic Compatibility Conference (GEMCCON)* (IEEE, 2016), p. 1–6
54. W. Park, H. Shin, B. Choi, W.-K. Rhim, K. Na, and D.K. Han, Advanced hybrid nanomaterials for biomedical applications. *Prog. Mater Sci.* 114, 100686 (2020).
55. E. Steen Redeker, D.T. Ta, D. Cortens, B. Billen, W. Guedens, and P. Adriaensens, Protein engineering for directed immobilization. *Bioconjug. Chem.* 24(11), 1761 (2013).
56. E. Polo, S. Puertas, M. Moros, P. Batalla, J.M. Guisán, J.M. Fuente, and V. Grazú, Tips for the functionalization of nanoparticles with antibodies, *Immobilization of Enzymes and Cells*. (Cham: Springer, 2013), pp. 149–163.
57. C.R. Borges and N.D. Sherma, Techniques for the analysis of cysteine sulfhydryls and oxidative protein folding. *Antioxidants Redox Signaling* 21(3), 511 (2014).
58. G. Yi, J. Son, J. Yoo, C. Park, and H. Koo, Application of click chemistry in nanoparticle modification and its targeted delivery. *Biomater. Res.* 22(1), 1 (2018).
59. V. Gascón, C. Márquez-Álvarez, I. Díaz, and R.M. Blanco, Hybrid ordered mesoporous materials as supports for permanent enzyme immobilization through non-covalent interactions, *Non-covalent Interactions in the Synthesis and Design of New Compounds*. (Hoboken: Wiley, 2016), pp. 345–360.
60. E. Kim and H. Koo, Biomedical applications of copper-free click chemistry: *in vitro*, *in vivo*, and *ex vivo*. *Chem. Sci.* 10(34), 7835 (2019).
61. Y. Liu, W. Hou, H. Sun, C. Cui, L. Zhang, Y. Jiang, Y. Wu, Y. Wang, J. Li, B.S. Sumerlin, Q. Liu, and W. Tan, Thiol–ene click chemistry: a biocompatible way for orthogonal bioconjugation of colloidal nanoparticles. *Chem. Sci.* 8(9), 6182 (2017).
62. Y. Takayama, K. Kusamori, and M.J.M. Nishikawa, Click chemistry as a tool for cell engineering and drug delivery. *Molecules* 24(1), 172 (2019).
63. X. Jiang, K. Abedi, and J. Shi, Polymeric nanoparticles for RNA delivery, *Reference Module in Materials Science and Materials Engineering*. (Amsterdam: Elsevier, 2021).
64. F. Lin, H.-R. Jia, and F.-G.J.M. Wu, Glycol chitosan: a water-soluble polymer for cell imaging and drug delivery. *Molecules* 24(23), 4371 (2019).
65. R. Serra-Gómez, J.M. Martinez-Tarifa, J. González-Benito, and G. González-Gaitano, Cyclodextrin-grafted barium titanate nanoparticles for improved dispersion and stabilization in water-based systems. *J. Nanopart. Res.* 18(1), 24 (2016). https://doi.org/10.1007/s11051-015-3321-x.
66. G. Ciofani, S. Danti, D. D'Alessandro, S. Moscato, M. Petrini, and A. Menciassi, Barium titanate nanoparticles: highly cytocompatible dispersions in glycol-chitosan and doxorubicin complexes for cancer therapy. *Nanoscale Res. Lett.* 5(7), 1093 (2010).
67. J. Čulić-Viskota, W.P. Dempsey, S.E. Fraser, and P. Pantazis, Surface functionalization of barium titanate SHG nanoprobes for *in vivo* imaging in zebrafish. *Nat. Protoc.* 7(9), 1618 (2012).
68. T. Jordan, M.A. O'Brien, C.-P. Spatarelu, and G.P. Luke, Antibody-conjugated barium titanate nanoparticles for cell-specific targeting. *ACS Appl. Nano Mater.* 3(3), 2636 (2020).
69. R.H. Huang, N.B. Sobol, A. Younes, T. Mamun, J.S. Lewis, R.V. Ulijn, and S. O'Brien, Comparison of methods for surface modification of barium titanate nanoparticles for aqueous dispersibility: toward biomedical utilization of perovskite oxides. *ACS Appl. Mater. Interfaces* 12(46), 51135 (2020).
70. S. Dong, J.-F. Li, and D. Viehland, Longitudinal and transverse magnetoelectric voltage coefficients of magnetostrictive/piezoelectric laminate composite: theory. *IEEE Trans. Ultrason. Ferroelectr. Freq. Control* 50(10), 1253 (2003).
71. I.T. Smith, E. Zhang, Y.A. Yildirim, M.A. Campos, M. Abdel-Mottaleb, B. Yildirim, Z. Ramezani, V.L. Andre, A. Scott-Vandeusen, P. Liang, and S. Khizroev, Nanomedicine and nanobiotechnology applications of magnetoelectric nanoparticles. *Wiley Interdiscip. Rev. Nanomed. Nanobiotechnol.* 15, e1849 (2022).
72. M. Acosta, N. Novak, V. Rojas, S. Patel, R. Vaish, J. Koruza, G.A. Rossetti, and J. Rödel, $BaTiO_3$-based piezoelectrics: fundamentals, current status, and perspectives. *Appl. Phys. Rev.* 4(4), 041305 (2017).
73. A.E. Miroshnichenko, A.B. Evlyukhin, Y.S. Kivshar, and B.N. Chichkov, Substrate-induced resonant magnetoelectric effects for dielectric nanoparticles. *ACS Photonics* 2(10), 1423 (2015).
74. A. Nagesetti, A. Rodzinski, E. Stimphil, T. Stewart, C. Khanal, P. Wang, R. Guduru, P. Liang, I. Agoulnik, J. Horstmyer, and S. Khizroev, Multiferroic coreshell magnetoelectric nanoparticles as NMR sensitive nanoprobes for cancer cell detection. *Sci. Rep.* 7(1), 1610 (2017).
75. O. Yalçın, *Ferromagnetic Resonance: Theory and Applications* (Norderstedt: BoD–Books on Demand, 2013).
76. D. Schwenk, F. Fishman, and F. Schwabl, Soft modes in ferroelectric superlattices. *Ferroelectrics* 104(1), 349 (1990).